Electronic Supplementary Information

Alkylaluminium Schiff base complexes derived from the dianilines [(2-$NH_2C_6H_4)_2X$] (X = O, CH_2CH_2): Synthesis, characterization and ROP capability.

Wenxue Yang,[a] Qe-King Zhao,[a] Timothy J. Prior,[b] David L. Hughes,[c] Abdessamad Arbaoui,[c] Mark R.J. Elsegood [d] and Carl Redshaw [a,b*]

[a] *College of Chemistry and Materials Science, Sichuan Normal University, Chengdu, 610066, China.*

[b] *Department of Chemistry, University of Hull, Hull, HU6 7RX, U.K.*

[c] *School of Chemistry, University of East Anglia, Norwich, NR4 7TJ, U.K.*

[d] *Chemistry Department, Loughborough University, Loughborough, Leicestershire, LE11 3TU, U.K.*

Contents

Figure S12. Packing in the structure of complex **10**.

Table S2. ROP of ε-caprolactone (runs 1 – 13) and *rac*-lactide (runs 14 – 23) by **1 - 14** (not **8 - 10**) for ε-CL and complexes **1** – **6** and **11- 14** for *rac*-lactide.

Figure S13 and **S14**. MALDI-ToF of PCL (runs 2 and 5, Table S2)

Figure S15. Plot of average molecular weight (M_n) *versus* conversion for PCL.

Figures S16 and S17. ^{1}H NMR spectra of the PCL (runs 2 and 5, Table S2)

Figure S18. ^{1}H NMR spectra of the PLA (run 4, Table 3; run 17, table S2)

Figure S19. MALDI-ToF of PLA (run 4, Tables 3; run 17 table S2)

Figures S20 and S21. 2D J-resolved ^{1}H NMR spectra of PLA (runs 2 and 5, Tables 3; runs 15 and 18, table S2).

Table S1. The 'Cleft'

The principal opposing C_6 rings that are closest to the centre of elliptical shape of the macrocyclic ring are the phenolate rings, and it is these rings that form the $\pi\cdots\pi$ contacts across the ring (in some compounds), etc. In the complexes analysed, the angles between opposing phenolate rings, with other data, are:

Compound	Angle between normals to phenolate ring planes /°	Angles between the C_6–C–N–C_6 groups /°	Dist. between the centroids of C1 and C25 rings /Å	Dist. between the centroids of C19 and C43 rings /°
L^1H_2·MeCN	89.03(5)/90.97(5)	74.93(3)	7.237	8.498
L^2H_2·MeCN, Mol A	12.56(12)	15.88(8)	3.897	8.846
L^2H_2·MeCN, Mol B	9.49(14)	21.96(8)	3.785	9.130
L^2H_2·2(Me_2CO)	7.39(7)	23.36(3)	3.869	9.704
L^2H_2·MeCOOEt	6.09(8)	17.87(2)	3.838	10.417
L^2H_2·2(MeCOOEt)	6.8(2)	34.76(10)	3.969	10.427
L^2H_2·2(PhMe)	89.88(7)	71.45(6)	6.795	7.710
L^2(tosyl)$_2$	0.0	0.0	4.965	-

Figure S1. Stacking of $\mathbf{L}^{1}H_2$ molecules parallel to the *c* axis.

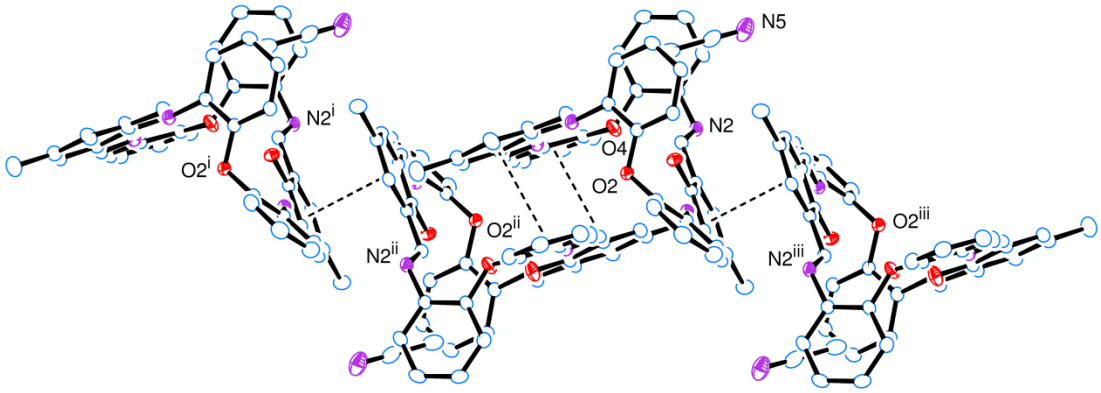

Figure S2. A general view of one molecule of $\mathbf{L}^{2}H_2$·MeCN, indicating the atom numbering scheme. The second molecule is similar. H atoms not involved in H-bonding and the two disordered MeCN molecules are omitted for clarity.

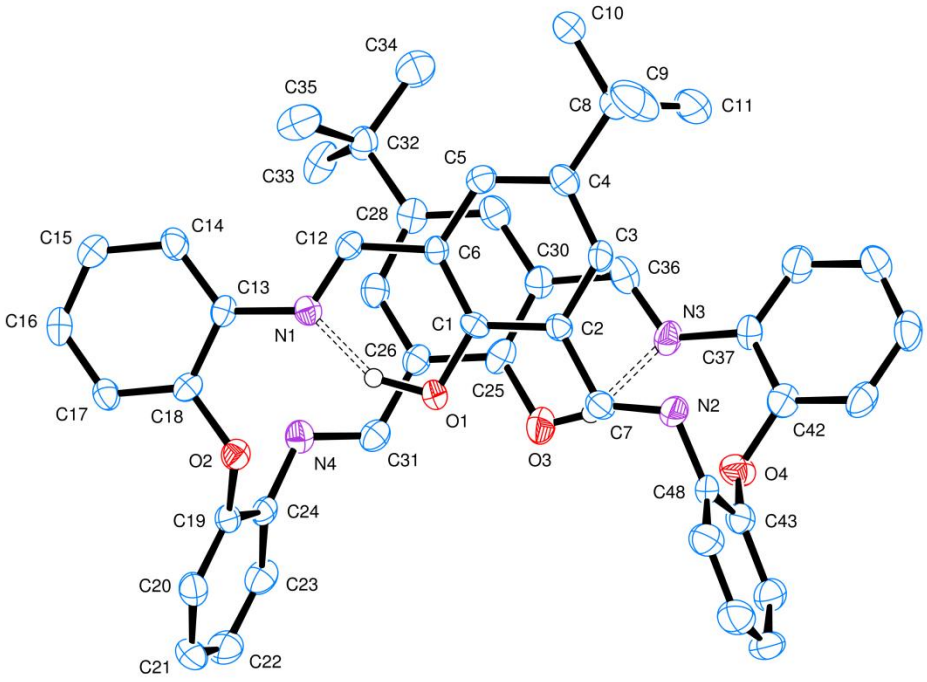

Figure S3. An 'end-on' view of one molecule of $\mathbf{L}^{2}H_2 \cdot$MeCN illustrating the sides of the cleft being almost parallel.

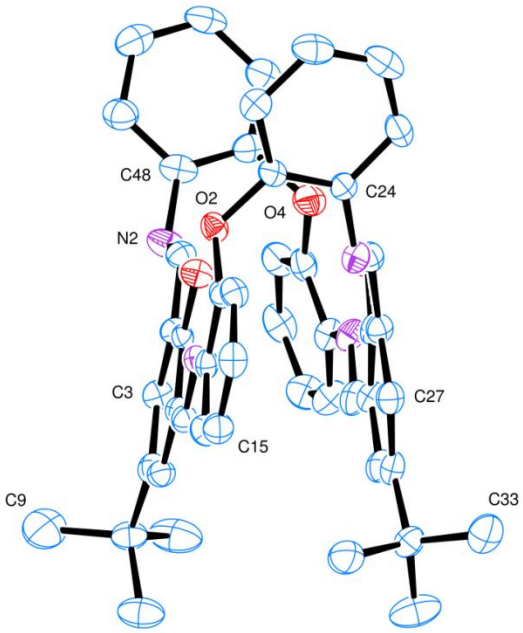

Figure S4. A view of a molecule of $\mathbf{L}^{2}H_2$·ethyl acetate, indicating the atom numbering scheme. H atoms not involved in H-bonding and the second disorder component of the ethyl acetate molecule are omitted for clarity.

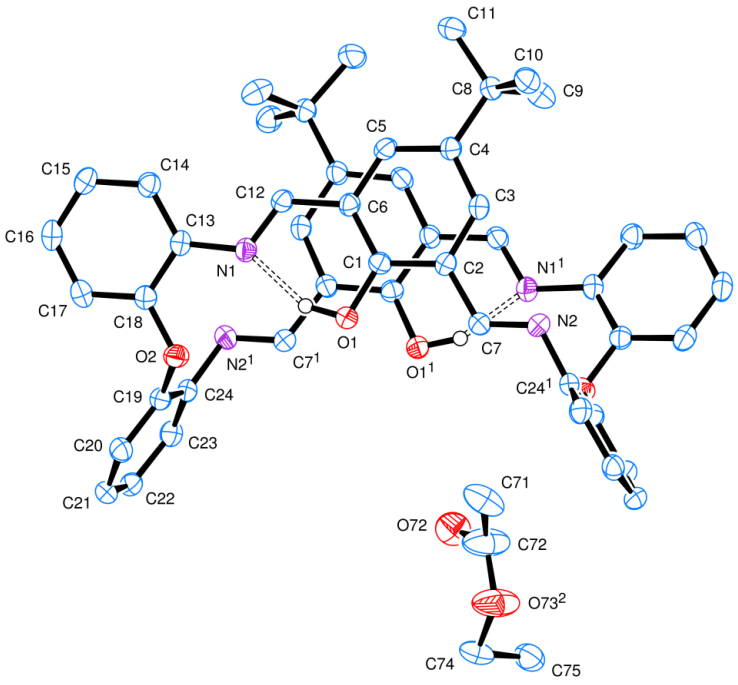

Figure S5. π···π interactions in $\mathbf{L^2}H_2 \cdot 2$ethylacetate (minor disorder components have been removed for clarity).

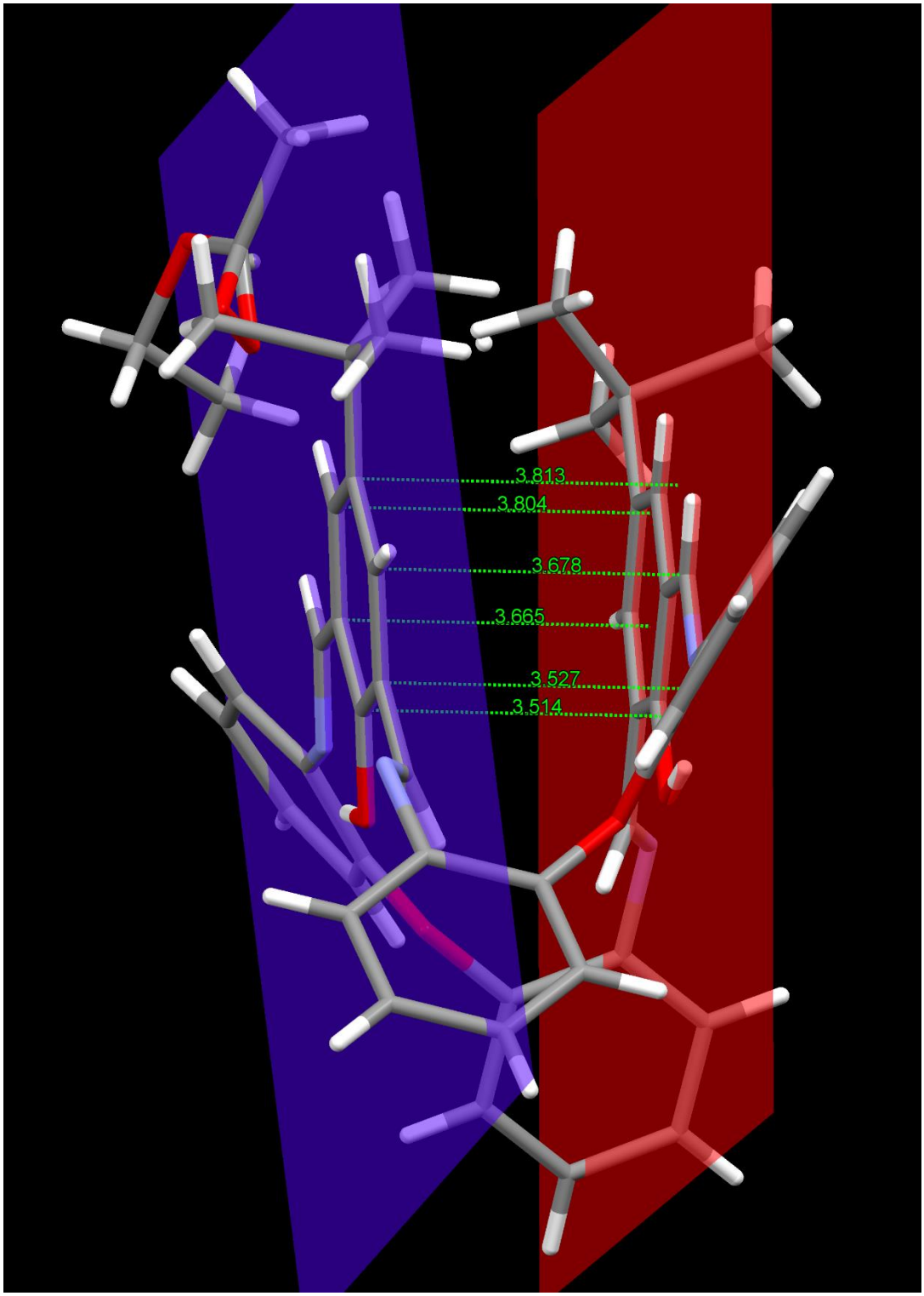

Figure S6. A view of one molecule of $\mathbf{L}^{2}H_2 \cdot 2$(acetone), indicating the atom numbering scheme. H atoms not involved in H-bonding have been omitted for clarity.

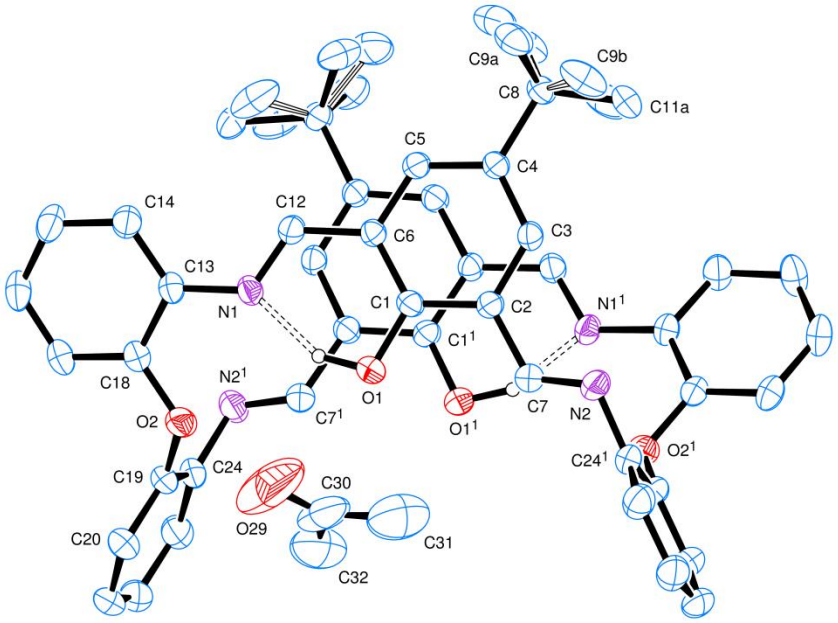

Figure S7. A view of a molecule of $\mathbf{L}^{2}H_2 \cdot 2$(toluene), indicating the atom numbering scheme. H atoms not involved in H-bonding have been omitted for clarity.

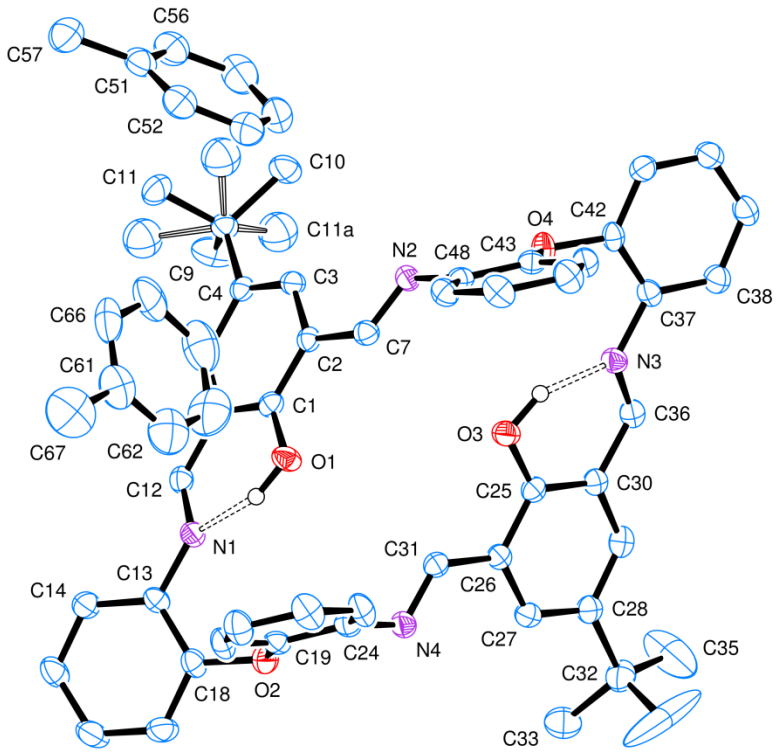

Figure S8. π···π interactions in $\mathbf{L^2}H_2 \cdot 2$toluene

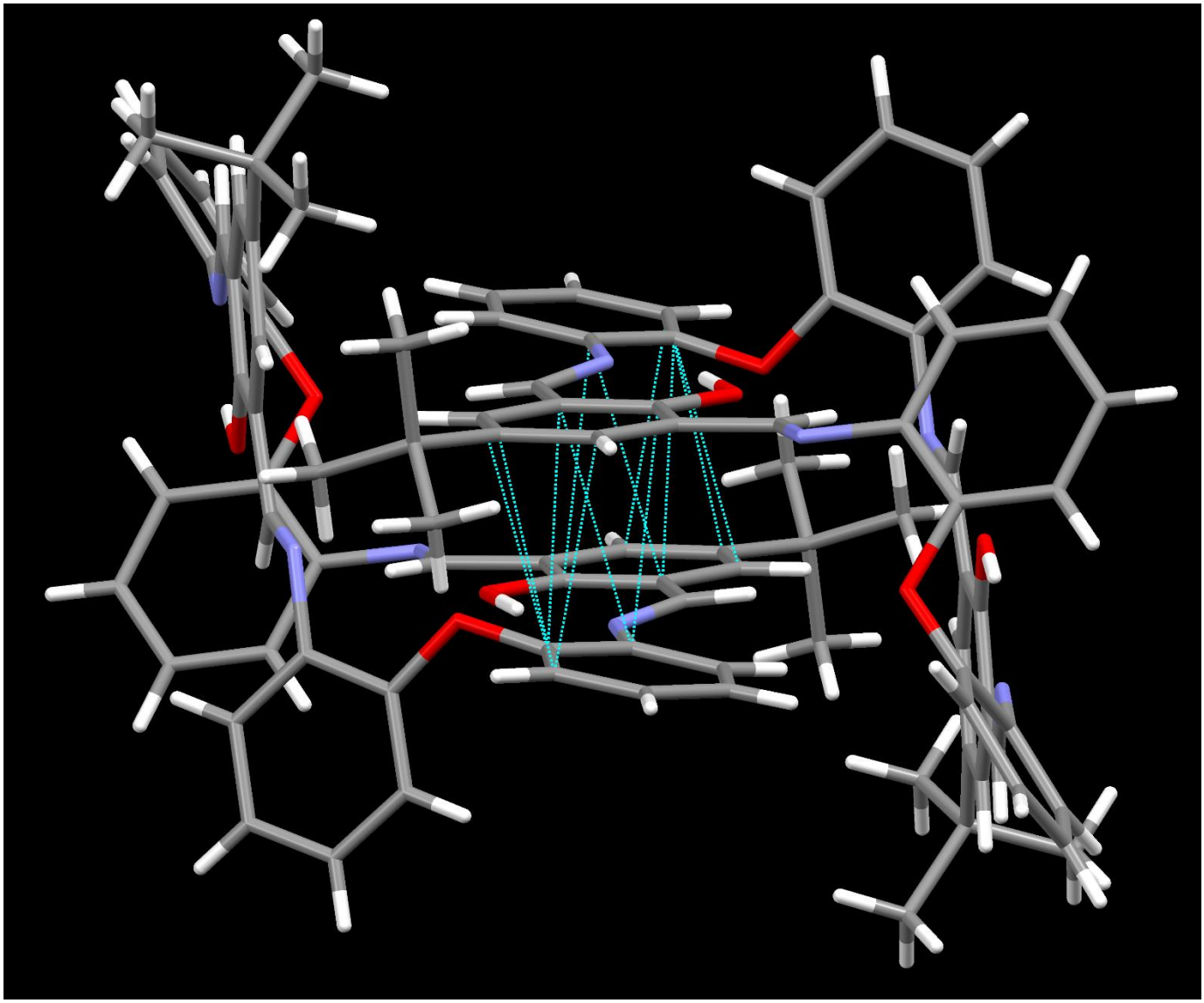

Figure S9. Molecular structure of $\mathbf{L^2}(tosyl)_2$. Selected bond lengths (Å) and angles (°): S(1)–O(51) 1.417(2), S(1)–O(52) 1.423(2), S(1)–O(1) 1.620(2), N(2)–C(7) 1.256(4), N(2)–C(24') 1.419(4), N(1)–C(12) 1.268(4), N(1)–C(13) 1.421(4); C(51)–S(1)–O(1) 105.14(14), N(2)–C(7)–C(2) 121.4(3), N(1)–C(12)–C(6) 120.0(3) °. H atoms have been omitted for clarity.

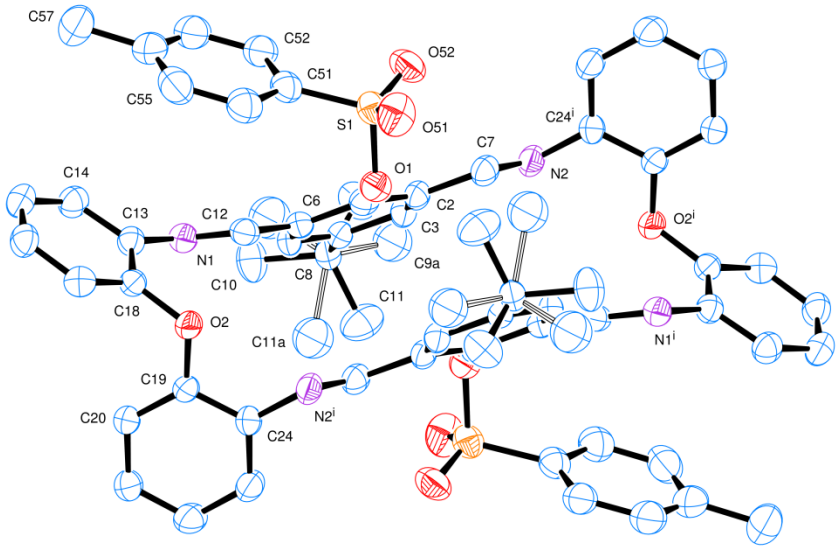

Figure S10. Alternative view of $\mathbf{L^2}(tosyl)_2$

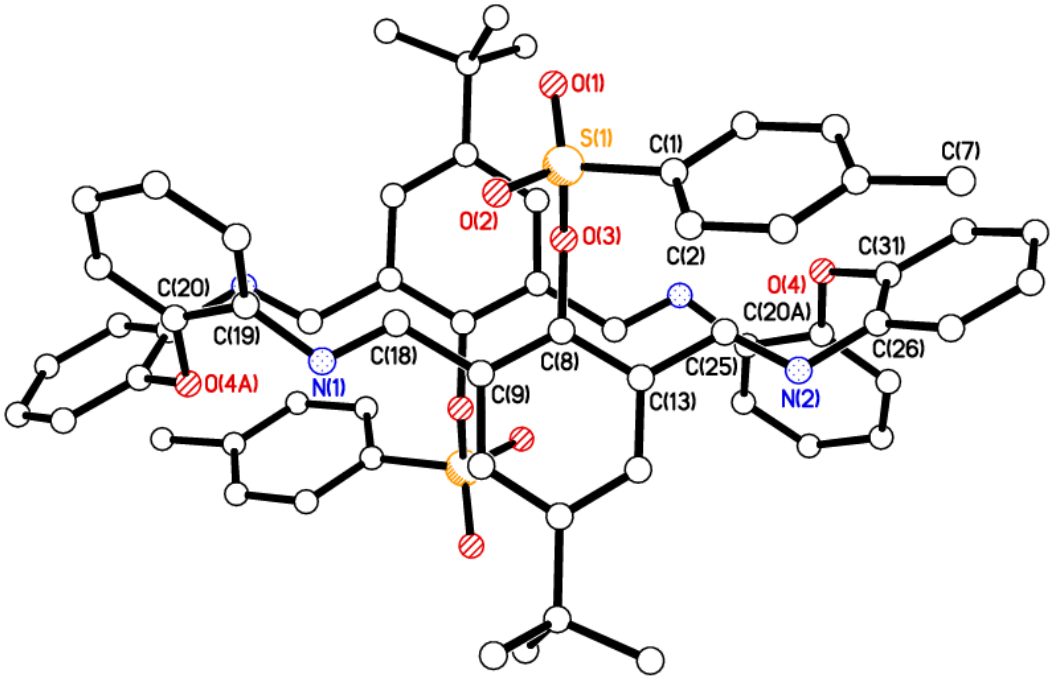

Figure S11. Alternative view of structure of complex **10**.

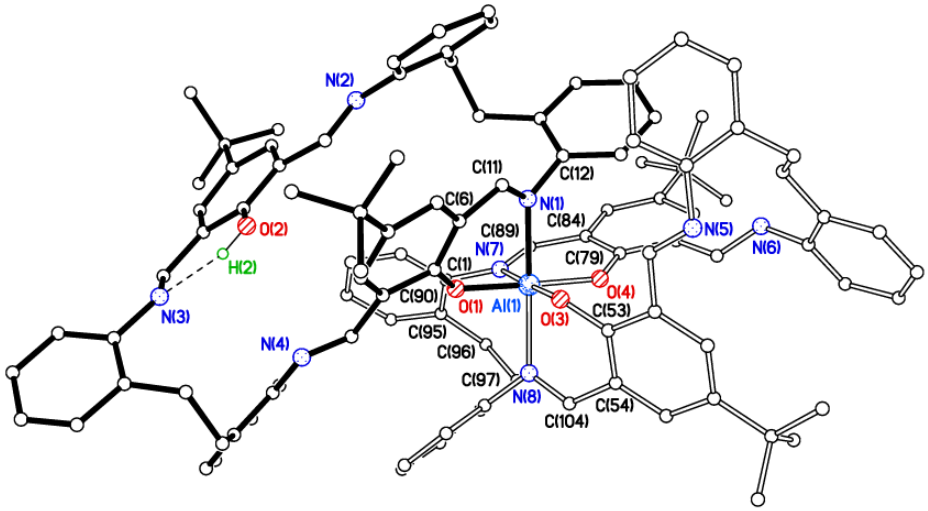

Figure S12. Packing in the structure of complex **10**.

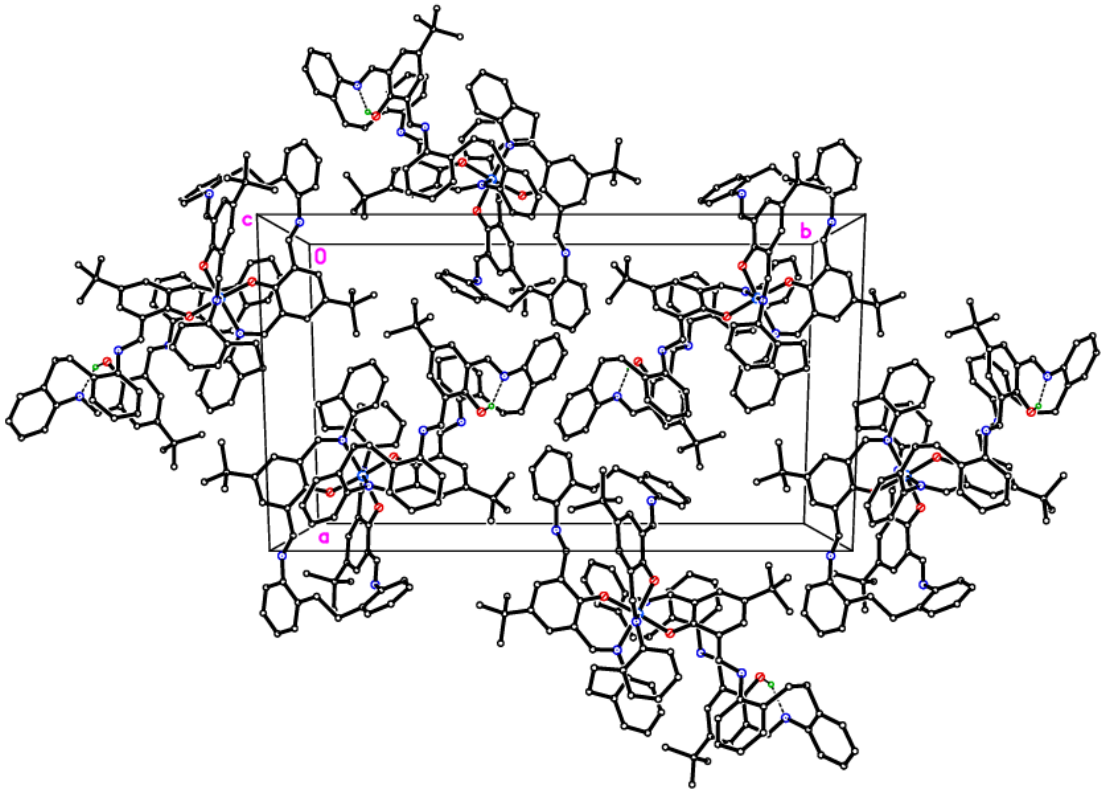

Table S2. ROP of ε-CL (runs 1 – 13) and *rac*-lactide (runs 14 – 23) using complexes **1-16** (not **8-10**) for ε-CL and complexes **1** – **6** and **11- 14** for *rac*-lactide.

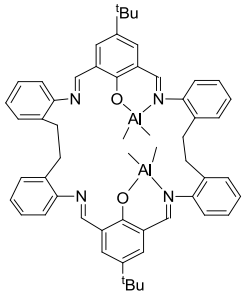

15

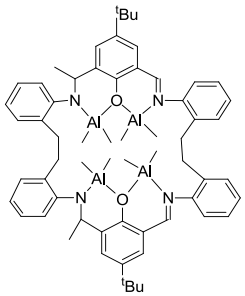

16

Run	Complex	CL/*rac*.LA: M: BnOH	T/℃	t/h	Conv./%[a]	M_n× $10^{4b, d}$	M_n Cal× 10^{4c}	PDI[e]
1	**1**	250:1:1	80	0.5	93.2	3.32	2.65	1.41
2	**2**	250:1:1	80	0.5	96.7	3.52	2.73	1.49
3	**3**	250:1:1	80	0.5	95.0	2.87	2.79	1.30
4	**4**	250:1:1	80	0.5	97.1	3.49	2.79	1.22
5	**5**	250:1:1	80	0.5	98.0	3.67	2.82	1.31
6	**6**	250:1:1	80	0.5	96.5	3.05	2.83	1.42
7	**7**	250:1:1	80	0.5	25.6	0.45	0.58	1.26
8	**11**	250:1:1	80	0.5	98.7	3.05	2.81	1.11
9	**12**	250:1:1	80	0.5	80.9	2.56	2.30	1.49
10	**13**	250:1:1	80	0.5	99.1	3.27	2.82	1.40
11	**14**	250:1:1	80	0.5	94.3	2.76	2.68	1.30
12	**15**	250:1:1	80	0.5	38.5	0.76	1.09	1.23
13	**16**	250:1:1	80	0.5	29.1	0.56	0.82	1.24
14	**1**	100:1:1	110	12	94.8	1.65	1.32	1.38
15	**2**	100:1:1	110	12	98.4	1.47	1.37	1.36
16	**3**	100:1:1	110	12	93.5	1.39	1.42	1.13
17	**4**	100:1:1	110	12	95.7	1.78	1.40	1.11
18	**5**	100:1:1	110	12	98.7	1.60	1.40	1.19
19	**6**	100:1;1	110	12	94.0	1.39	1.42	1.12

20	**11**	100:1:1	110	12	97.6	1.41	1.40	1.31
21	**12**	100:1:1	110	12	95.3	1.23	1.36	1.23
22	**13**	100:1:1	110	12	96.5	1.41	1.38	1.10
23	**14**	100:1:1	110	12	93.2	1.13	1.34	1.07

[a] By ^{1}H NMR spectroscopic analysis. [b] For ε-CL, obtained from GPC analysis times 0.56.[c] (F.W.[M]/[BnOH])(conversion). [d] For *rac*-lactide, M_n values were determined by GPC in THF *vs* PS standards and were corrected with a Mark-Houwink factor of 0.58. [e] Polydispersity index (M_w/M_n) were determined by GPC.

Figure S13 and **S14**. MALDI-ToF of PCL (runs 2 and 5, table S2)

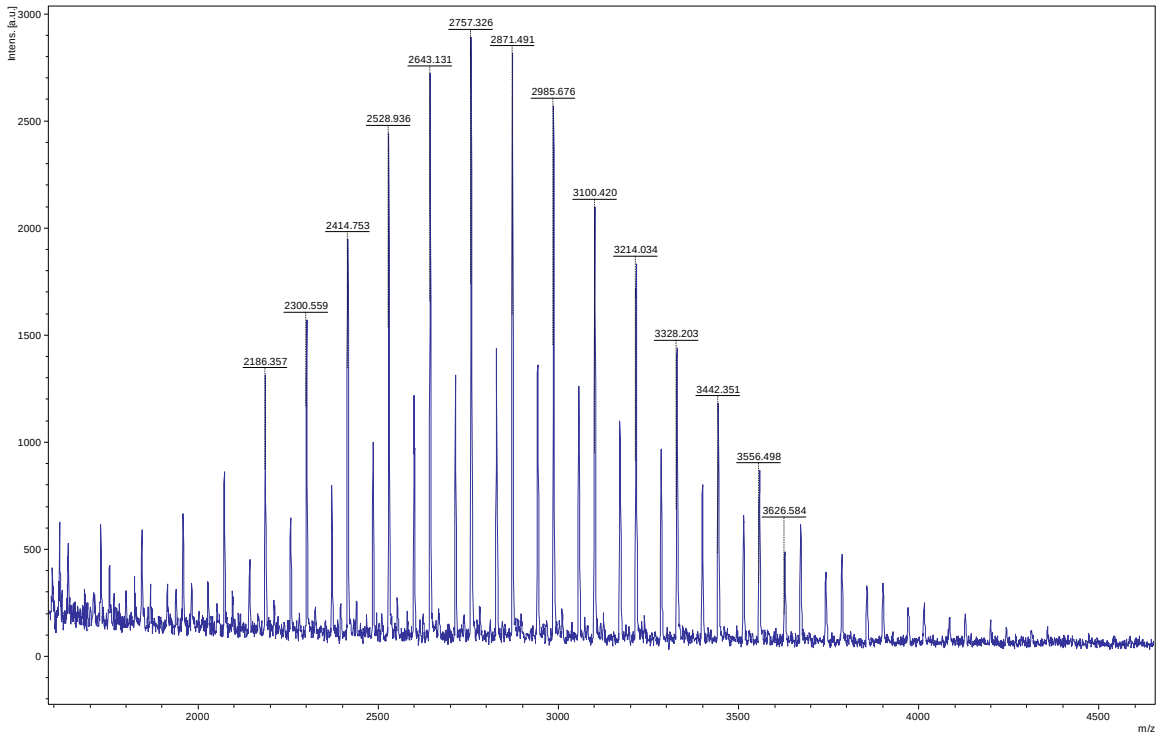

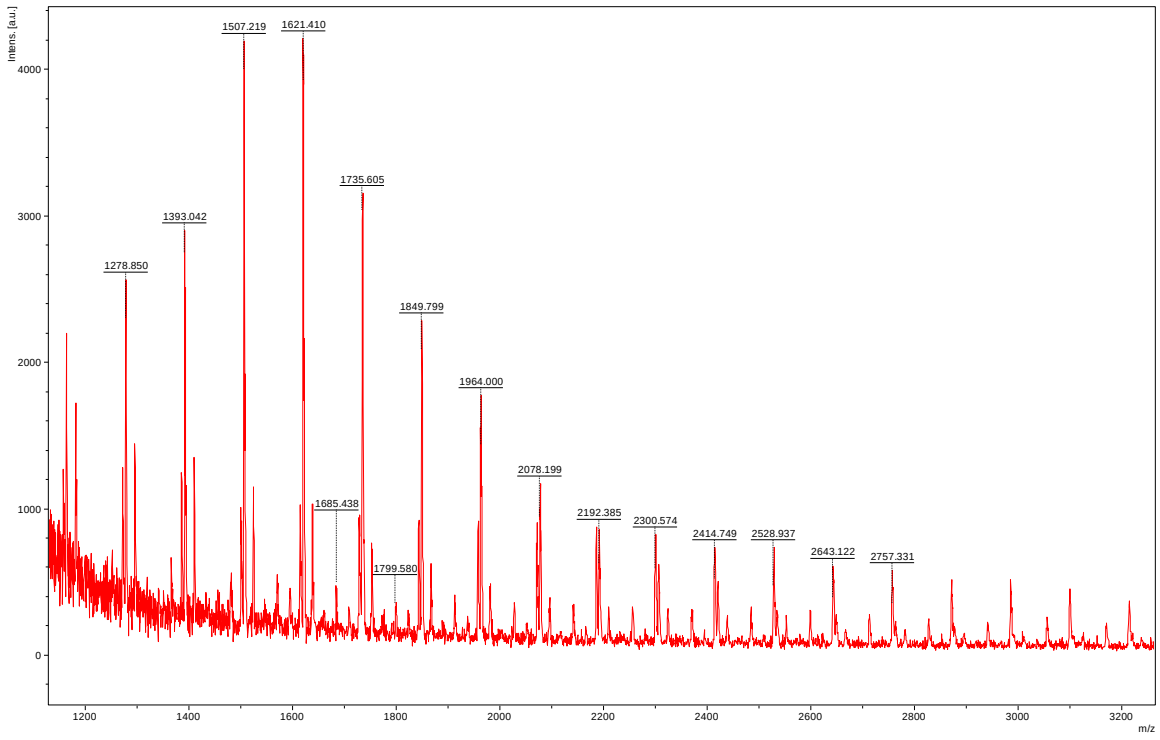

Figure S15. Plot of average molecular weight (M_n) *versus* conversion for PCL.

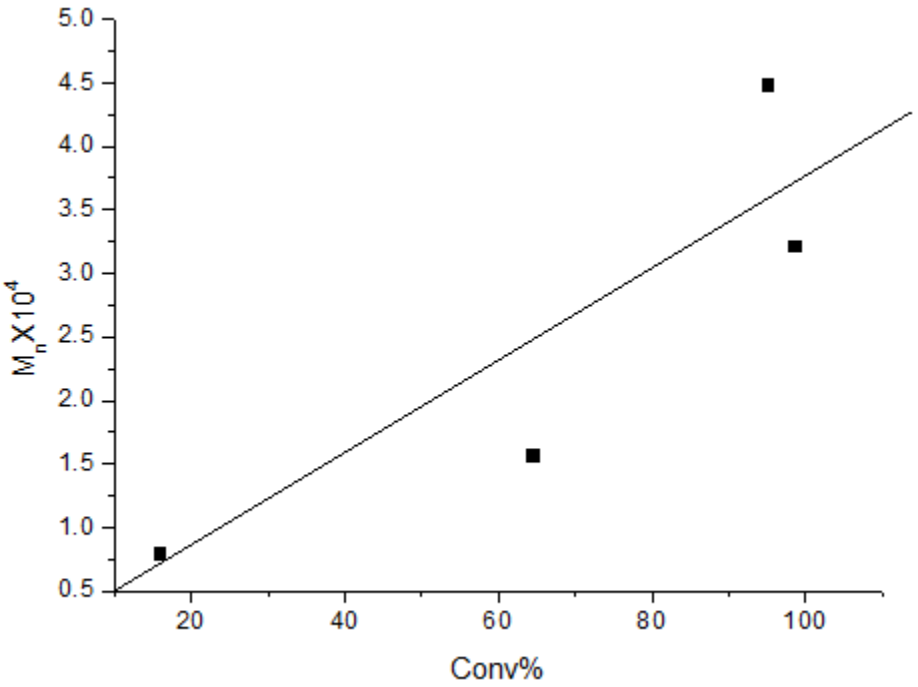

Figures S16 and S17. ^{1}H NMR spectra of the PCL (runs 2 and 5, table S2)

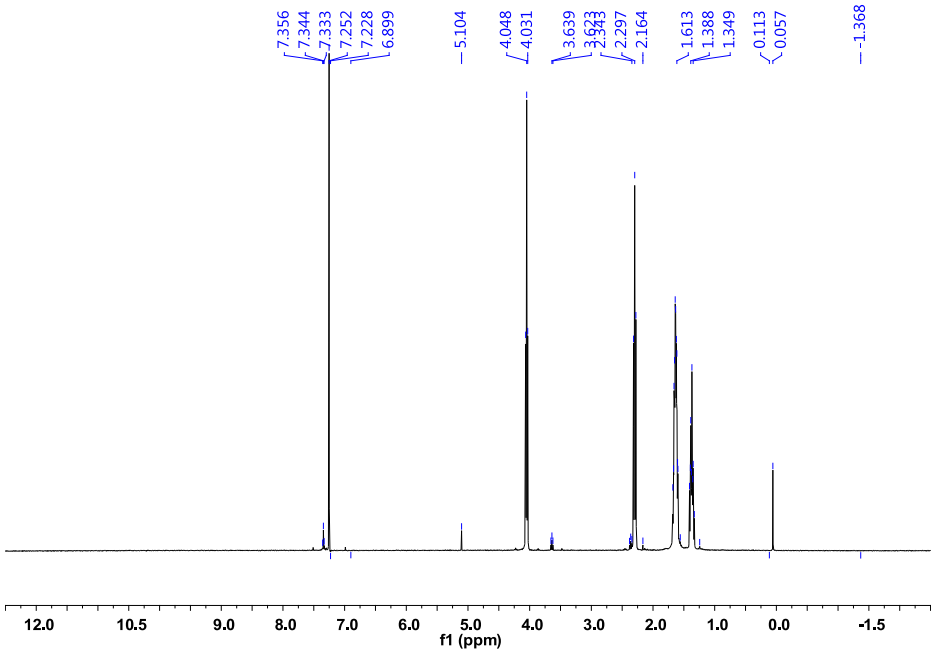

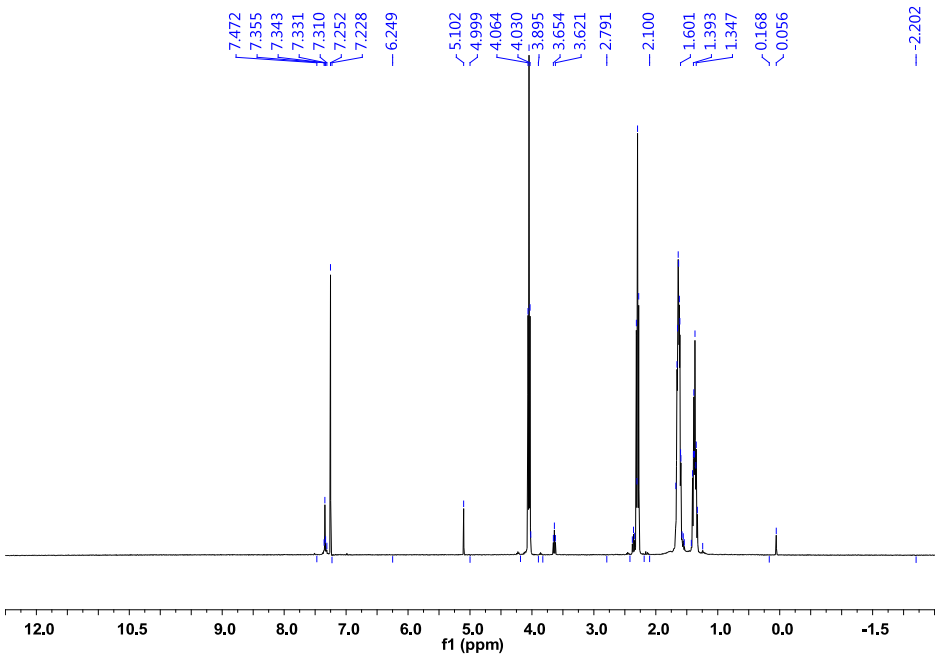

Figure S18. ^{1}H NMR spectra of the PLA run 4, Tables 3 (run 17 table S2).

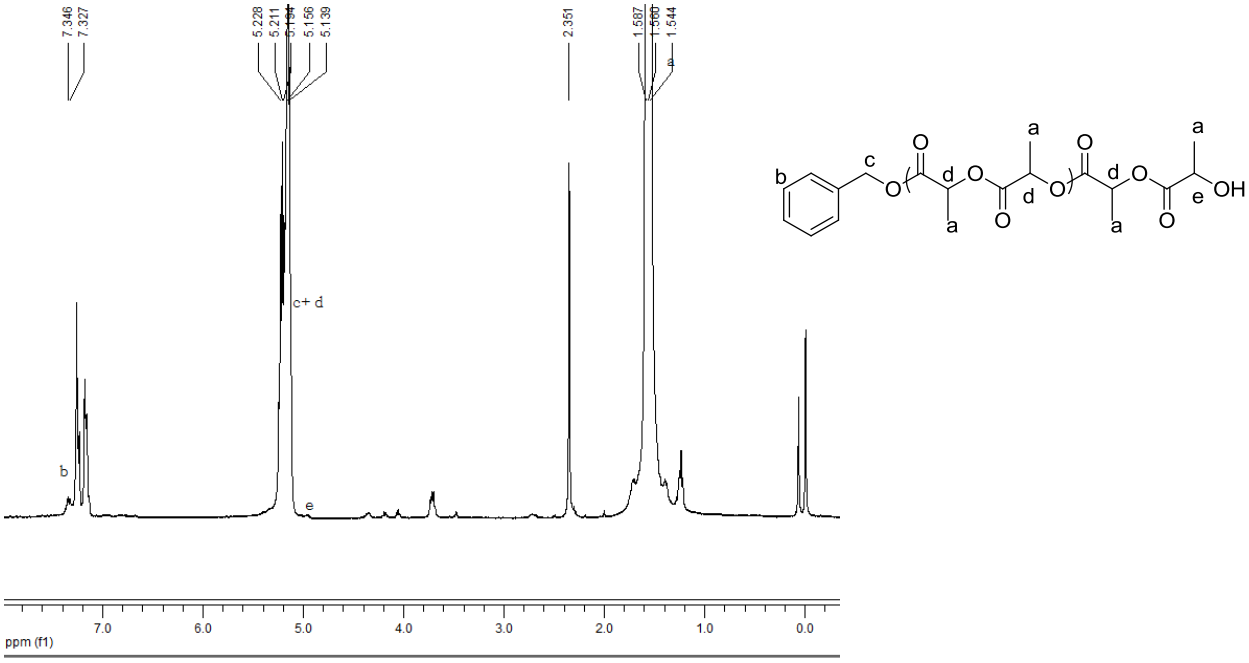

Figure S19. MALDI-ToF of PLA run 4, Table 3 (run 17 table S2)

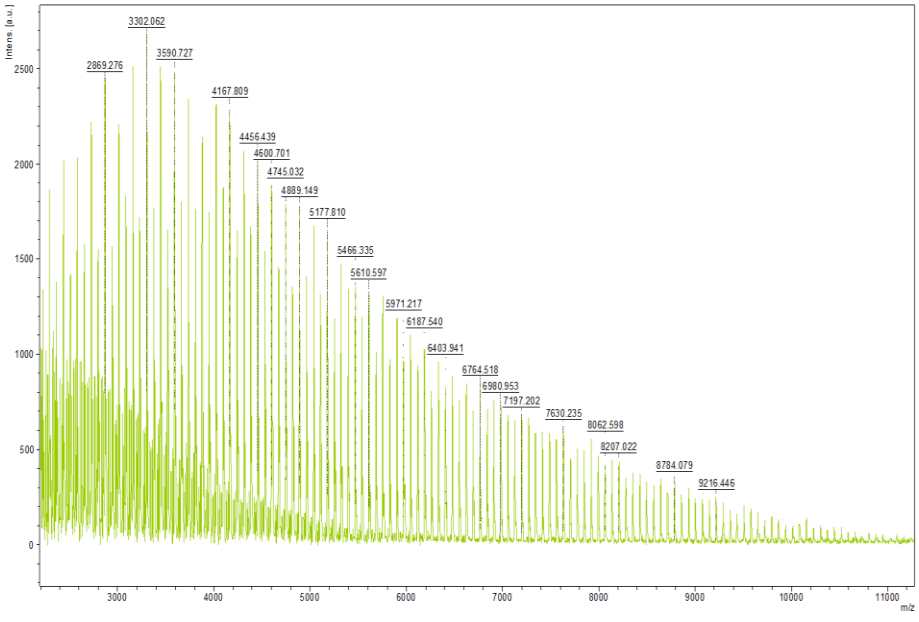

Figures S20 and **S21**. 2D J-resolved ^{1}H NMR spectra of PLA , runs 2 and 5, Tables 3 (runs 15 and 18, table S2).

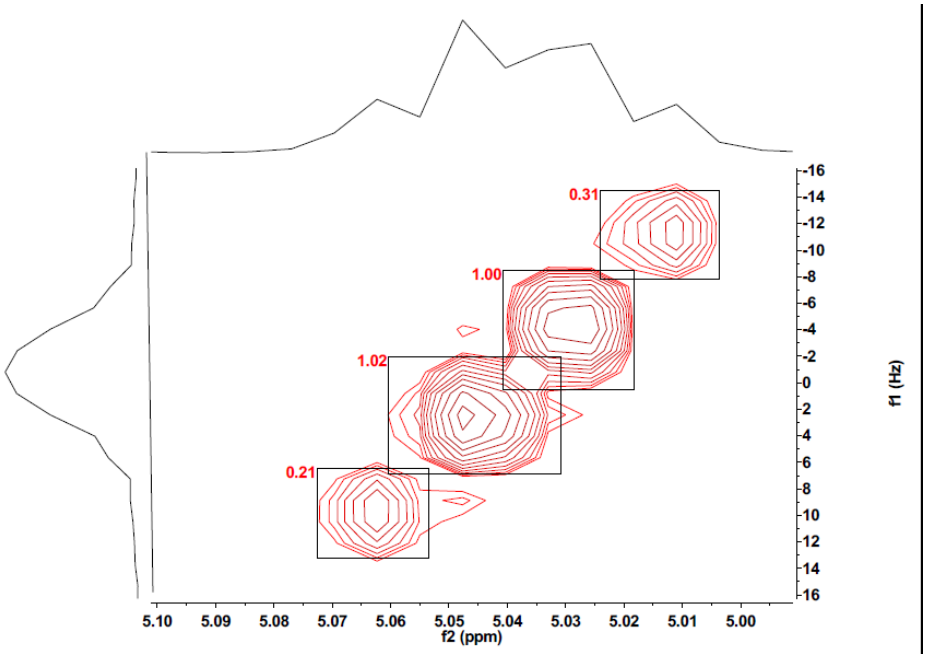

Run 2
Pr = (2* [rmr])$^{1/2}$
Pr= 0.64

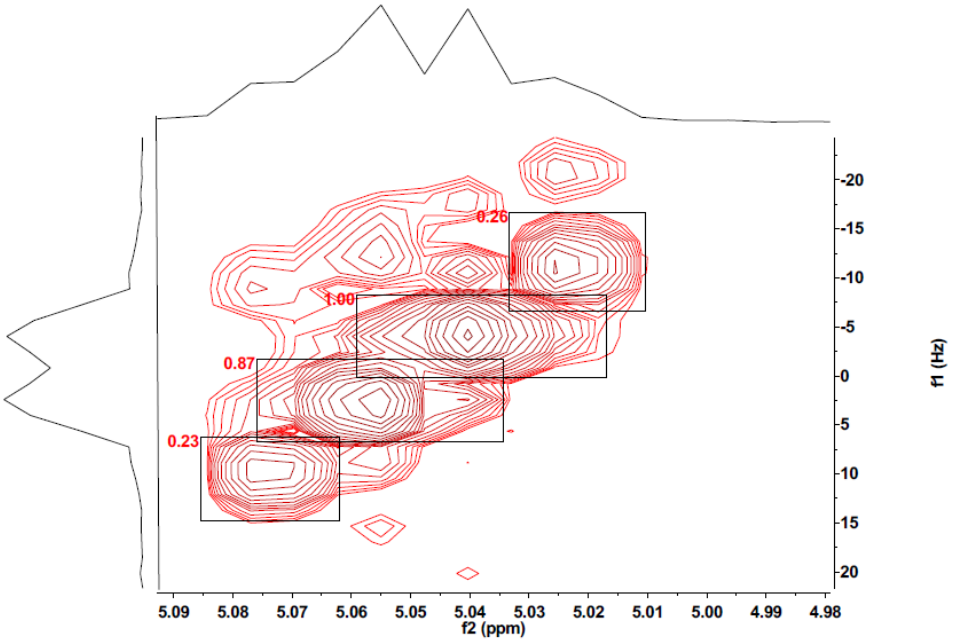

Run 5
Pr = 0.67